

Dispersionless motion in a driven periodic potential

S. Saikia¹ and Mangal C. Mahato*

Department of Physics, North-Eastern Hill University, Shillong-793022, India

¹*Department of Physics, St. Anthony's College, Shillong-793001, India.*

(Dated: February 13, 2022)

Recently, dispersionless (coherent) motion of (noninteracting) massive Brownian particles, at intermediate time scales, was reported in a sinusoidal potential with a constant tilt. The coherent motion persists for a finite length of time before the motion becomes diffusive. We show that such coherent motion can be obtained repeatedly by applying an external zero-mean square-wave drive of appropriate period and amplitude, instead of a constant tilt. Thus, the cumulative duration of coherent motion of particles is prolonged. Moreover, by taking an appropriate combination of periods of the external field, one can postpone the beginning of the coherent motion and can even have coherent motion at a lower value of position dispersion than in the constant tilt case.

PACS numbers: : 05.10.Gg, 05.40.-a, 05.40.Jc, 05.60.Cd

The inertial Brownian particle motion in periodic potentials[1, 2] has been an archetypal model to theoretically understand many phenomena in physical systems. The current-voltage characteristics of (RCSJ model of) Josephson junctions[3], the electrical conductivity of superionic solids[4], motion of adatoms on the surface of a crystal[5], etc., are some of the important examples[1]. However, not all behaviour of the model particle motion in all time regimes are exhaustively investigated. A recent example being the discovery of dispersionless particle motion in a tilted periodic potential in the intermediate time regime by Lindenberg and coworkers[6]. During the coherent motion, the ensemble averaged position dispersion, $\Delta x(t) = \langle (x(t) - \langle x(t) \rangle)^2 \rangle$, remains constant.

This interesting phenomenon is shown (numerically) by particles moving on a cosinusoidal potential with a constant tilt (CT), F_0 , in a medium with constant friction coefficient γ_0 [6] in a limited (F_0, γ_0) region. The particles, after crossing the immediate barrier move (after $t = \tau_1 > \tau_K$, the Kramers mean passage time) coherently with velocity $v \approx \frac{F_0}{\gamma_0}$. The coherent motion continues until it is overwhelmed (at around $t = \tau_2$) by the diffusive motion of the particles. τ_1 and τ_2 are specified only as a rough guide[6]. In this work we investigate the effect of a zero-mean square-wave external drive (ZMSW) $F(t)$ of half period τ and amplitude F_0 , instead of a CT.

The coherent motion, naturally, gets interrupted upon reversal of direction of F at $t = \tau$ ($\tau_1 < \tau < \tau_2$). Interestingly, as a main result of this work, the coherent motion once disturbed, by reversing the field at $t = \tau$, gets reestablished around $t = \tau + \tau_1$ in almost the same form as it was during $\tau_1 < t < \tau_2$ in the CT case. And this loss and subsequent recovery of coherent motion continues for a large number of reversals of $F(t)$. The dispersion $\Delta x(t)$, however, increases rapidly during $\tau < t < \tau + \tau_1$. (During $0 < t < \tau_1$, $\Delta x(t) \sim t^\alpha$, $\alpha \approx 2$).

We consider the motion of an ensemble of Brownian particles each of mass m moving in a potential $V(x) = -V_0 \sin(kx)$ in a medium with friction coefficient[7] $\gamma(x) = \gamma_0(1 - \lambda \sin(kx + \phi))$ at temperature T (in units of k_B) and subjected to an external force field $F(t)$. The corresponding Langevin equation in dimensionless form is given by[8]

$$\frac{d^2x}{dt^2} = -\gamma(x)\frac{dx}{dt} + \cos x + F(t) + \sqrt{\gamma(x)T}\xi(t), \quad (0.1)$$

with $\gamma(x) = \gamma_0(1 - \lambda \sin(x + \phi))$. Here all terms are written in units of m , V_0 and k , for example, the scaled time t is measured in units of $\sqrt{\frac{m}{V_0 k^2}}$, etc. The Gaussian distributed zero-mean random forces $\xi(t)$ satisfy $\langle \xi(t)\xi(t') \rangle = 2\delta(t - t')$. The applied square-wave force $F(t)$ is taken as $F(t) = \pm F_0$ for $(2n\tau \leq t < (2n+1)\tau)$ and $F(t) = \mp F_0$ for $((2n+1)\tau \leq t < (2n+2)\tau)$ with $n = 0, 1, 2, \dots$. For constant applied force $F(t) = F_0$ (for all t) the equation is solved using the matrix continued fraction method and also numerically, supporting each other quantitatively[1, 9, 10, 11, 12]. However, for finite τ , the equation could be solved only numerically. The integration of the equation, using the 4th order Runge-Kutta method[13], was carried out in time steps of $\Delta t = .001$.

We take $\lambda = 0.9$. $\lambda \neq 0$, however, is relevant only while discussing ratchet current at the end. In fact, except for this minor point, all the results discussed in the following qualitatively remain same for the simpler case of $\lambda = 0$.

The particles exhibit coherent motion in the potential $V(x) = -\sin(x) - xF_0$, in the intermediate times roughly in the range $[\tau_1 (\approx 2 \times 10^3) < t < \tau_2 (\approx 3 \times 10^4)]$, for $F_0 = 0.2$. Therefore, we choose the ZMSW field $F(t)$ of amplitude $F_0 = 0.2$ and, in most cases, half period $\tau = 5000$ which is well within the range $[\tau_1, \tau_2]$. Naturally, in the first half period ($0 < t \leq \tau$) the motion is same as in the CT case. In all cases, we take the initial ($t = 0$) particle position distribution as $\delta(x - \frac{\pi}{2})$ and Maxwell velocity distribution corresponding to $\bar{T} = 0.4$. Note that after every half period τ the periodic potential gets tilted in the reversed direction as a result of field reversal.

*Electronic address: mangal@nehu.ac.in

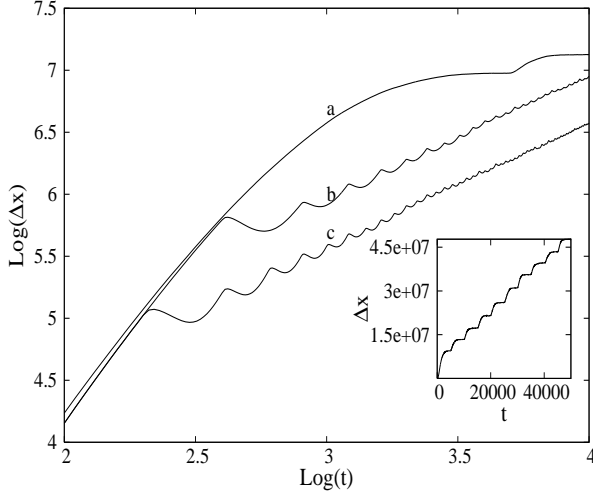


FIG. 1: The position dispersion $\Delta x(t)$ for $\tau = 5000$ (a), 400 (b), and 200 (c) are plotted. The Inset shows curve (a) extended to 10 half periods.

Fig.1, curve (a) and its extended plot in the Inset show that by applying the field, $F(t)$, with $\tau = 5000$ a repetitive sequence of trains of coherent motion, with characteristic constant $\Delta x(t)$ is obtained. These bursts of coherent motion are quite robust. Each burst of coherent motion is preceded by a length of dispersive particle motion. As a result $\Delta x(t)$ grows, in discrete steps, with time, as the number n of half periods increases.

The generation of coherent motion continues for many ($n \gg 8$) half periods ($\tau = 5000$) of $F(t)$, Inset of Fig.1. Thus, as an important consequence, the cumulative duration ($\approx n(\tau - \tau_1)$) of coherent motion when driven by $F(t)$ is made much larger than the duration, $\tau_2 - \tau_1$, achievable in the CT case.

In the Fig.1 are also plotted Δx corresponding to the half periods $\tau = 400$ (curve (b)), and 200 (curve (c)). The important feature to be noticed in the figure is that, for $\tau = 400, 200 < \tau_K, \tau_1$, Δx dips immediately after the field is reversed before it rises. This behaviour of dispersion dipping and subsequent rise becomes most pronounced at a small but intermediate τ . It continues for many periods of $F(t)$.

Fig.2, summarizes the main results of this work. It shows many interesting effects of taking few initial half periods of $F(t)$ of smaller duration, $\tau = 400$ (curve (b)), and $\tau = 200$ (curves (c-d)) and then making its later half periods $\tau = 5000$ or larger (e.g., 10000, curve (d)). The curves (b-c) show that, in this case too, during the later half periods $\tau = 5000$ of $F(t)$, a similar sequence of trains of coherent motion, as in Fig.1, Inset (or curve (a)), can be obtained. It also allows to postpone (curve (b)) the appearance of coherent motion beyond $t = \tau_1$. Moreover, it is possible to obtain coherent motion with lower constant dispersion (curves (c,d)) than in the CT case (i.e., lower than the constant Δx in the first half period in the curve (a)) too. Curve (e) shows that the

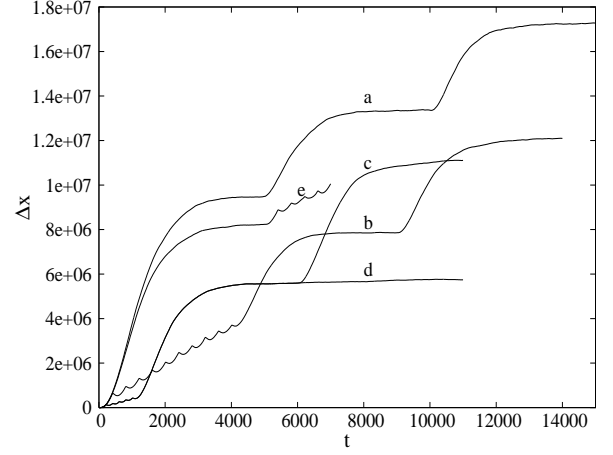


FIG. 2: $\Delta x(t)$ for three $\tau = 5000$ (a) ten $\tau = 400$ and two $\tau = 5000$ (b), five $\tau = 200$ and two $\tau = 5000$ (c), five $\tau = 200$ and one $\tau = 10000$ (d), and one $\tau = 5000$ and five $\tau = 400$ (e) half periods are plotted.

curves (b-d) can be repeated, using the same customized procedure, many times over again.

The results of Figs.1 and 2 can be understood by analyzing the time evolution of velocity distribution, $P(v)$. $P(v)$ at various phases of $F(t)$ at $t = 5\tau$, and at $t = \tau + 15.6$ for $\tau = 5000$ and at $t = 2\tau$, and $t = 2\tau + 16$ for $\tau = 1000$ are shown in Fig.3. $P(v)$ invariably assumes almost a Gaussian form of same width and centred at a fixed $v \approx \pm \frac{E_0}{\gamma_0}$ at $t = n\tau$ for $\tau = 5000$. The Inset, showing the mean velocity $\bar{v}(t)$ and velocity dispersion $\Delta v(t)$, supports this observation. However, at $t = n \times 1000$, $P(v)$ has two peaks one centred at $v \approx \pm \frac{E_0}{\gamma_0}$ and the other at $v = 0$.

The $P(v)$ peak at $v = 0$ shows that at $t = n\tau$, for $\tau < \tau_1$, some particles are left behind in the locked state in one or some other wells. The smaller is τ more prominent this latter peak is left at $t = \tau$. These locked particles try to gravitate to their respective well bottoms and, being slower, even succeed in shrinking the position distribution $P(x)$ more effectively than the much faster particles in the running state on the front. Thus, for smaller $\tau < \tau_1$, the bimodal nature of $P(v)$ helps appreciable Δx dipping immediately after field reversal, Fig.1.

At $t = n\tau + t_0$, $15 < t_0 < 16$, \bar{v} becomes zero for all τ , and n . (It turns out, $2\tau_0 \approx \frac{m}{\gamma_0}$.) The corresponding $P(v)$ are also shown in Fig.3. For $\tau = 5000$, $P(v)$ at $t = n\tau + t_0$ is like a sum of two "Gaussians" centred on either side of $v = 0$. But for $\tau = 1000$, the surviving $P(v)$ peak at $v = 0$ at $t = n\tau$, contributes an additional one centred at $v = 0$, making $\bar{v} = 0$ at the same delay time τ_0 .

Due to the tilt direction reversal the particles, in the running state, are forced to reverse their direction of motion and hence each of them necessarily go through zero velocity at least once momentarily. Thus, the entire system passes approximately through a "thermal" state at $t = n\tau + \tau_0$. Hence, after every field reversal at $t = n\tau$ the

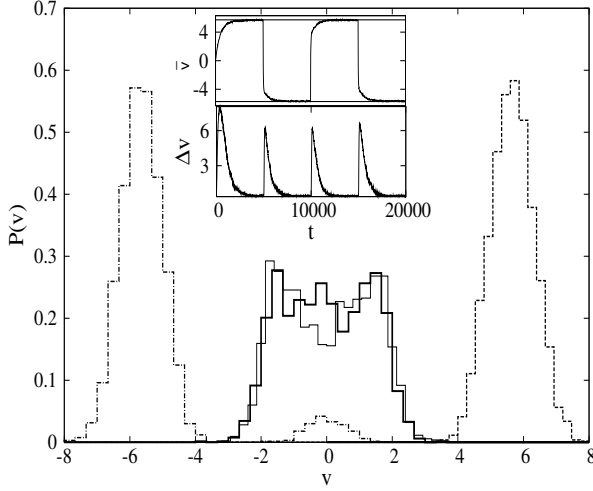


FIG. 3: $P(v)$ at $t = 25000$ (right peak) and at 25015.6 (middle thin line) for $\tau = 5000$, and at $t = 2000$ (bimodal), at 2016 (middle bold line) for $\tau = 1000$. $\bar{v}(t)$, and $\Delta v(t)$ for $\tau = 5000$ are plotted ($\bar{v} = \pm F_0/\gamma_0$ lines drawn) in the Inset.

particles begin their subsequent journey in the reversed direction with almost the same delayed initial condition (at $t = n\tau + \tau_0$) of thermalized $P(v)$. Therefore, Δx are expected to behave similarly after every $n\tau$.

As discussed above, it is just the reversal of field which leads $P(v)$ to the required form at $t = n\tau + t_0$, irrespective of the form of $P(v)$ at $t = n\tau$ for any value of $\tau \gg \tau_0 \approx 16$. It shows that in order to obtain coherent motion neither an exact initial Gaussian velocity distribution is necessary nor all the particles are required to be initially confined sharply to a single well bottom of the periodic potential. Also, a mere switching the field alternately *on* ($F_0 \neq 0$) for duration τ and *off* ($F_0 = 0$) for the same duration τ , fails to yield results like Figs.1 and 2. This indicates that a reversal of the field direction is essential because this alone ensures a "thermalized" $P(v)$.

It must also be noted that during the CT case the average particle displacement is large, $\approx \frac{\tau_2 F_0}{\gamma_0}$ by the end of its coherent motion whereas in the ZMSW case it is zero, for $\lambda = 0$, and small and finite for $\lambda \neq 0$ and $\phi \neq 0, \pi$ after any large time $t = 2n\tau$. This is an added practical advantage over the CT case for, in the ZMSW case, most of the particles on the average remain confined to a finite region of space despite periodically showing coherence of motion for a long time.

The dimensionless values of parameters used (e.g., $\gamma_0 = .035$, $T = .4$, $\tau = 5000$, and $F_0 = .2$) and other derived quantities when restored to their usual units are presented in Table 1 for three illustrative cases: (i) The motion of an Ag ion in AgI crystal[14], (ii) the motion of a macromolecule (kinesin) along a polymer fibre (microtubule)[15], and (iii) diffusion of Cooper pairs across a Josephson junction[3]. Notice that $\omega (= \frac{\gamma_0}{m}) \ll \omega_0$, in the particle motion case, and $\omega \ll \omega_P$, the Josephson plasma frequency ($= \frac{2eI}{\hbar C}$), showing that the

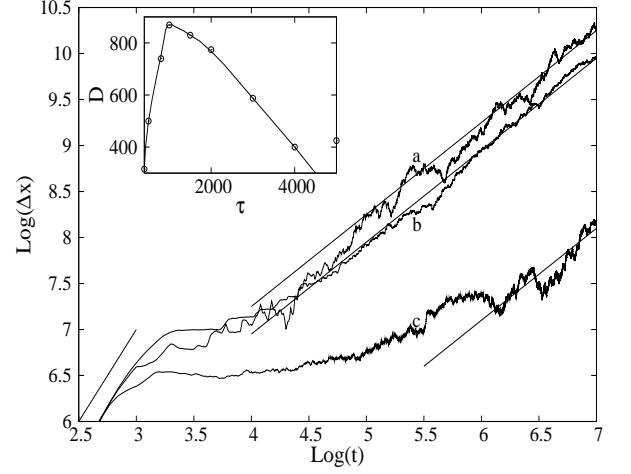


FIG. 4: $\Delta x(t)$ for $\tau = 1000$ (a), 5000 (b), and for the case of CT $F_0 = 0.2$ (c) averaged over, respectively, 20, 60, and 18 ensembles are plotted. Lines of slope 1 are fitted to the curves. The short line at the lower left corner indicates $\Delta x \sim t^\alpha$, $\alpha \approx 2$. The inset shows variation of D with τ .

systems considered are, indeed, underdamped. The last column of the Table gives the magnitude of mean velocity (mean voltage) attained during the coherent state when the initial value of the drive field $F(t)$ ($I(t)$) is fixed either at $+|F_0|$ ($+|I_0|$) or with their sign reversed and not an equal mixture of both. Also, during the half period τ the particles move to an average distance (the product of quantities in the last two columns) of the order of a micron (μ) which will get retraced in the next half period. This gives a rough idea of the sample size one would need to take in a ZMSW case. Also, $\frac{2\pi}{\tau} \ll \omega_0 (\omega_P)$ (by about two orders of magnitude).

The calculated average velocities \bar{v} and velocity dispersions Δv are plotted, in the Inset of Fig.3. An equal mixture of $F(t = 0) = \pm |F_0|$ makes \bar{v} close to zero during coherent motion. It is exactly zero for $\lambda = 0$ at all t and hence even in the limit $t \rightarrow \infty$ \bar{v} remains zero. However, for $\lambda \neq 0$ and $\phi \neq 0, \pi$ a nonzero finite mean (steady state) velocity is obtained[10, 11, 12] earlier. The contribution of coherent particle motion being insignificant, the dispersive motion alone contributes to this *ratchet* current of particles.

The diffusion constant, D , defined as $\lim_{t \rightarrow \infty} \Delta x(t) = 2Dt$, is hard to calculate for a constant tilt F_0 [6]. The asymptotic limit barely reaches even by $t = 10^7$. However, for ZMSW this limit is readily reached by $t = 10^7$, Fig.4. It may be noted that for each curve in Figs.1 and 2 we have averaged over 2000 realizations but in Fig.4 we could average over number of realizations ranging only between 18 and 60. The nature of $\Delta x(t)$ so clear in Fig.1 appears less convincing in Fig.4. Therefore, it is hard to conclude that the same nature of Δx , as in Fig.1, will continue till the asymptotic time regime. However, from the "thermalized" $P(v)$ argument given earlier, there is a fair likelihood that the nature of $\Delta x(t)$ shown in Fig.1

TABLE I: The systems considered are: (1) Ag: Ag on AgI lattice, (2) Mm: a macromolecule along a polymer, and (3) JJ: Josephson junction. The symbols have their usual meaning. The RCSJ-model JJ equation equivalent to Eq.(2.1) is[3]:

$$\frac{\hbar C}{2e} \frac{d^2\theta}{dt^2} + \frac{\hbar}{2e} G(1 + \lambda \cos(\theta + \phi)) \frac{d\theta}{dt} + I_1 \sin(\theta) = I(t) + \sqrt{2TG(1 + \lambda \cos(\theta + \phi))} \xi(t). \quad (\text{Add } -\frac{\pi}{2} \text{ to } \theta \text{ for exact correspondence.})$$

	$m(\text{Kg})$	$V_0(\text{eV})$	$T(\text{K})$	$k(\text{m}^{-1})$	$\omega_0(\text{s}^{-1})$	$\gamma_0(\text{Kg s}^{-1})$	$\frac{\gamma_0}{m}(\text{s}^{-1})$	$F_0(\text{N})$	$\tau(\text{s})$	$\bar{v} = \frac{F_0}{\gamma_0}(\text{ms}^{-1})$
Ag	1.79×10^{-25}	0.15	348	$0.5\pi \times 10^{10}$	4.07×10^{12}	2.55×10^{-14}	1.42×10^{11}	5.03×10^{-10}	1.23×10^{-9}	1.48×10^3
Mm	3.32×10^{-22}	0.13	300	$2.5\pi \times 10^8$	6.20×10^9	7.21×10^{-14}	2.17×10^8	3.25×10^{-13}	8.06×10^{-7}	4.51×10
JJ	C	I_1	T	$\frac{2e}{\hbar}$	ω_P	G	$\omega = \frac{G}{C}$	I_0	τ	$\bar{V} = \frac{I_0}{G}$
	0.5 pF	10^{-9} Amp	9.53 mK	3.038×10^{15} $\text{V}^{-1}\text{s}^{-1}$	2.46×10^9 s^{-1}	4.31×10^{-5} Ohm^{-1}	8.63×10^7 s^{-1}	2.0×10^{-8} Amp	2.03×10^{-6} s	4.64×10^{-4} V

will extend to a large number of half periods of $F(t)$ provided a large number of particles are considered for averaging.

The nature of $\Delta x(t)$ shown by the curves in Figs.1, 2 is in no finite region close to $\Delta x(t) \sim t$. It remains, therefore, open to explain why a large number of repeatedly same diverse combinations of dispersions such as ones ranging from $\Delta x(t) \sim t^2$ to $\Delta x(t) \sim t^0$, when averaged over a large number of realizations, yields the same nature of dispersion, $\lim_{t \rightarrow \infty} \Delta x(t) \sim t$, for all τ , Fig.4.

$D(\tau)$, plotted in the Inset of Fig.4, are rough estimates as the averagings are done only over a small number of realizations. However, the overall qualitative trend of $D(\tau)$ remains valid. $D(\tau)$ shows a peak around $\tau = \tau_1$. For $\tau > \tau_1$, the closer τ is to τ_1 smaller is the constant Δx region and hence larger is the fraction of sharply rising Δx region. Naturally total Δx will be larger as $\tau \rightarrow \tau_1$. However, the nature of $D(\tau)$ as $\tau \rightarrow \tau_2$ is not clear from the available data. In the range $\tau < \tau_1$, Δx rises only after an appreciable dipping, Fig.1. Therefore, the initial rise of Δx is slower as τ is decreased from τ_1 resulting in a smaller total $\Delta x(t)$ as $t \rightarrow \infty$ and hence smaller D .

From the *rms* spread ($\sqrt{\Delta x}$) point of view the advantage of ZMSW $F(t)$ over CT, except in cases like curve (d) in Fig.2, quickly evaporates as t increases. Whereas (for an Ag particle) at $t = 10\tau = 12.3 \times 10^{-9}\text{s}$ for the CT (ZMSW) case, the mean displacement \bar{x} is 1.8μ (≈ 0) and

$\sqrt{\Delta x} = .14\mu$ ($.40\mu$), at $t = 2.46 \times 10^{-6}\text{s}$ the corresponding numbers are $\bar{x} = 3.64\text{mm}$ (≈ 0) and $\sqrt{\Delta x} = .77\mu$ (6.08μ). Perhaps in the ZMSW case, the particles left behind during a τ get pushed farther away during the next τ , make the $\sqrt{\Delta x(t)}$ increase faster as t increases.

Coherent motion is observed only in the negative slope region of $D(\tau)$. However, for this same system it is shown in Ref.[12] that ratchet current is maximum for a value of $\tau \simeq 500$, i.e., in the rising $D(\tau)$ region and becomes significantly small for larger $\tau \geq \tau_1$ and almost zero at $\tau = 5000$. The peak of the $D(\tau)$, thus, roughly divides τ into two regions: (i) small τ giving ratchet current, and (ii) larger τ showing coherent motion.

To summarise, the dispersionless (coherent) motion discovered earlier, to occur for a brief but finite duration in the intermediate time regime, on a CT sinusoidal potential, was extended to the case of periodically reversing constant tilts. We have shown the possibility of obtaining coherent particle motion interspersed by dispersive motion over many periods of an external ZMSW field. The cumulative duration of coherent motion can, thus, be extended to a substantial fraction of the total journey time, of course, at a cost of making the system several times more diffusive.

MCM acknowledges support from the Abdus Salam ICTP, Trieste, where the paper was finalized.

-
- | | |
|--|--|
| <p>[1] H. Risken, <i>The Fokker-Planck Equation</i>, (Springer-Verlag, Berlin), 1996.</p> <p>[2] P. Reimann, Phys. Rep. 361, 57 (2002); R.P. Feynman, R.B. Leighton, and M. Sands, <i>The Feynman Lectures in Physics</i> (Publishers, year), Vol. 1, Chap. 46.</p> <p>[3] C.M. Falco, Am. J. Phys. 44, 733 (1976); A. Barone, and G. Paterno, <i>Physics and Applications of the Josephson Effect</i>, John Wiley, New York, 1982.</p> <p>[4] P. Fulde, L. Pieternero, W.R. Schneider, and S. Strässler, Phys. Rev. Lett. 35, 1776 (1975).</p> <p>[5] A.M. Lacasta, J.M. Sancho, A.H. Romero, I.M. Sokolov, and K. Lindenberg, Phys. Rev. 70, 051104 (2004).</p> <p>[6] K. Lindenberg, J.M. Sancho, A.M. Lacasta, and I.M. Sokolov, Phys. Rev. Lett. 98, 020602 (2007).</p> <p>[7] G. Wahnström, Surf. Sci. 159, 311 (1985).</p> <p>[8] A.M. Jayannavar, and M.C. Mahato, Pramana-J. Phys. 45 369 (1995); M.C. Mahato, T.P. Pareek, and A.M. Jayannavar, Int. J. Mod. Phys. B10, 3857 (1996).</p> | <p>[9] H. Risken, and H.D. Volmer, Z. Physik B 33, 297 (1979).</p> <p>[10] W.L. Reenbohn, S. Saikia, R. Roy, and M.C. Mahato, Pramana J. Phys. 71, 297 (2008).</p> <p>[11] W.L. Reenbohn, and M.C. Mahato, J. Stat. Mech: Theor. Exp. P03011 (2009).</p> <p>[12] S. Saikia, and M.C. Mahato, J. Phys.: Condens. Matter 21, 175409 (2009).</p> <p>[13] W.H. Press, S.A. Teukolsky, W.T. Vetterling, and B.P. Flannery, <i>Numerical Recipes (in Fortran): the Art of Scientific Computing</i>, Cambridge University Press, Cambridge, 1992; M.C. Mahato, and S.R. Shenoy, J. Stat. Phys. 73, 123 (1993).</p> <p>[14] M. Hayana, A. Hatate, and M. Oguni, J. Phys.: Condens. Matter 15, 3867 (2003).</p> <p>[15] R.D. Astumian, and M. Bier, Phys. Rev. Lett. 72, 1766 (1994).</p> |
|--|--|